

Article | Received 29 November 2024; Accepted 9 April 2025; Published 29 April 2025  
<https://doi.org/10.55092/sc20250008>

# Knowledge-based intelligence method for controlling segment floating by optimizing shield tail grouting parameters

Gan Wang, Qian Fang\*, Jun Wang, Guoli Zheng, Qiming Li and Jianying Wei

Key Laboratory of Urban Underground Engineering of Ministry of Education, Beijing Jiaotong University, Beijing 100044, China

\* Correspondence author; E-mail: [qfang@bjtu.edu.cn](mailto:qfang@bjtu.edu.cn).

## Highlights:

- A knowledge-based method is proposed to control segment floating in tunneling.
- The model captures active-passive parameter interplay and spatial-temporal features.
- A multi-rings optimization strategy resolves conflicts across adjacent ring sections.

**Abstract:** Extensive segment floating will result in segment dislocation, crack, and leakage, posing significant risks of engineering accidents. It is important to control the segment floating based on adjusting shield operational parameters finely. A knowledge-based intelligence method designed for controlling segment floating is proposed in this study. Leveraging prior knowledge in segment floating, the framework of the intelligence method is constructed. This framework consists of a segment floating prediction model along with two auxiliary models. The segment floating prediction model considers the spatial and temporal characteristics of the shield operational parameters, including the early activation of the shield excavation parameters and the hysteretic nature of tail grouting parameters. The segment floating prediction model is the basis of the knowledge-based intelligence method. A multi-ring optimization strategy is designed to solve the conflict between the optimization results of adjacent rings. The case study shows that the segment floating prediction model has high prediction accuracy due to consideration of the spatial and temporal characteristics of the shield operational parameters. Considering the performance and computation cost, the optimal parameter configuration is figured out.

**Keywords:** segment floating; shield tunnel; optimization; shield operational parameters

## 1. Introduction

Shield tunnelling is widely used in urban tunnel construction due to its priorities in construction speed, security, and automatization compared to other construction methods. In shield tunnelling construction, there are two indicators paid much attention to ensure construction safety: surface settlement and segment floating. Large cross-section tunnels or tunnels in water-rich strata are always subject to great



Copyright©2025 by the authors. Published by ELSP. This work is licensed under Creative Commons Attribution 4.0 International License, which permits unrestricted use, distribution, and reproduction in any medium provided the original work is properly cited.

buoyancy which will cause segment floating [1]. Extensive segment floating will result in segment dislocation, crack, and leakage and may even lead to engineering accidents. So, the control of segment floating is significant for ensuring the construction safety of shield tunnelling.

Many analytical solutions based on the limit equilibrium method or Terzaghi pressure formula are established to analyze the segment floating in different conditions. In analytical solutions, the segment floating is tightly related to the calculations of buoyancy and vertical load. Considering the soil arching effect, Geng *et al.* calculated the vertical load of the overlying soil [2]. Liu and Yuan investigated the influence of the dilation effect of sands on the floating resistance based on the limit equilibrium method [3]. Although the calculation of the analytical method is easy, the related factors considered in the analytical method are generally limited. Those methods are more suitable for the design phase of tunnels. In the construction phase, the engineer tends to inject a greater volume of grouting material at the top of the segment, while injecting minimal grouting material at the bottom, as a measure to mitigate segment floating. So, the analysis solution based on buoyancy calculation seldom acquires satisfactory results.

Generally, during shield tunnelling, the factors related to the segment floating are divided into two categories: tail grouting and attitude control [2]. Bezuijen *et al.* measured grouting pressure during shield tunnelling and studied the influence on buoyance force and bending moment in the lining [4]. Talmon and Bezuijen investigated the consolidation process of shield grouting and established an analytical model based on field monitoring data [5]. Jin *et al.* investigated the influence of the synchronous grouting and thrust on the segment floating based on the field test [6]. The optimization of synchronous grouting material is studied [7]. Jiang *et al.* presented a comprehensive review of the development and progress of synchronous grouting materials [8]. Liang *et al.* studied the distribution law of grouting material along the segment ring, the distribution of grouting material is tightly related to the lateral earth pressure, foundation reaction, grout shear stress, and gravity [1,7,9,10]. As for attitude control, Mei *et al.* argued that the uneven jack forces are applied to realize shield attitude control and contribute to the segment floating [11]. Jiang *et al.* suggested that segment floating can be effectively controlled by adjusting the shield excavation parameters and tunneling attitude [8]. Although existing literature give some simple strategies for controlling segment floating, the determination of proper shield operational parameters mostly relies on the engineering experience of shield operators in practice. Consequently, it is necessary to establish an intelligence model capable of solving the optimal shield operational parameters in terms of segment floating.

In recent years, machine learning and deep learning have been developed rapidly [12–26]. Based on deep learning, data-driven models are widely used in solving complicated engineering problems. Fang *et al.* proposed an intelligent back analysis method for the equivalent top loading curve of a pile [14]. Wang *et al.* proposed physics-informed a neural network aimed at estimating earth pressure [27]. Owing to the automation in the shield machine, shield tunnelling is more compatible with deep learning compared to other tunnel construction methods. Wang *et al.* proposed a deep-learning based prediction for the maximum settlement caused by single tunnel construction [28]. Ge *et al.* developed a data-driven model that predicts the ground surface settlement and segment floating simultaneously. In previous literature, few models focus on intelligence methods for segment floating prediction and optimization [29]. Moreover, existing intelligent methods have exhibited a deficiency in incorporating prior knowledge about segment floating.

In this study, we propose a knowledge-based intelligence method for controlling segment floating by adjusting and optimizing shield tail grouting parameters. Drawing upon prior knowledge in segment

floating control, we establish a comprehensive framework for the intelligence method, comprising a primary model and two auxiliary models. The primary model serves as a segment floating prediction model, while the two auxiliary models predict torque, thrust, and grouting pressure, respectively. The segment floating prediction model accounts for the intricate interplay among active control and passive response parameters, leveraging geometrical, geological, and shield operational parameters to predict segment floating behavior accurately.

In this paper, we proposed a knowledge-based intelligence method for controlling segment floating based on adjusting and optimizing shield tail grouting parameters. Based on prior knowledge in controlling segment floating, we construct the framework of the intelligence method, comprising a main model and two auxiliary models. The main model serves as a segment floating prediction model, while the two auxiliary models are the torque and thrust predicting model and the grouting pressure predicting model, respectively. The segment floating prediction model considers the intricate interplay between active control and passive response parameters, leveraging geometrical, geological, and shield operational parameters to predict segment floating behavior accurately. The segment floating prediction model also considers the spatial and temporal characteristics of the shield operational parameters, including the early activation of the shield excavation parameters and the hysteretic nature of tail grouting parameters. To address the conflicts between the optimization results of adjacent rings, a multi-rings optimization strategy is developed. The influence of the optimization algorithms and the multi-rings optimization strategy is investigated with filed data.

## 2. Mechanism of segment floating

### 2.1. Process of segment floating

During shield tunnelling, the segments are assembled within the shield machine and subsequently released from the shield machine tail. Because there is an annular gap between the surrounding soil and the outer surface of the released segment, tail grouting is used to compensate the gap. The segment tends to move upward after being released from the shield machine tail, and the upward movement is generally called segment floating. During shield tunnelling, there are many factors related to the segment floating. Sometimes, the segment moves downwards due the complex factors. Noted, the upward and downward movements are both referred to as segment floating in this work.

The process of segment floating can be divided into three stages as shown in Figure 1. Stage I initiates upon the completion of the assembly of the segment, and ends with the segment's release from the shield machine tail. Stage II ends with the full consolidation of the grouting material surrounding the segment. In Stage I, theoretically, it is imperative for the shield machine to be aligned with the designated tunnel axis. However, it is impossible to maintain accurate orientation all the time, leading to a permissible deviation of the shield tunnel from the designed tunnel axis within specified limits. Generally, the actual orientation of the shield machine is represented by the pitching angle as shown in Figure 1. The misalignment between the jack and its nearest segment results in a vertical component of the jack force. When the shield machine tilts downward, the segment is subjected to an upward force, leading to the segment floating.

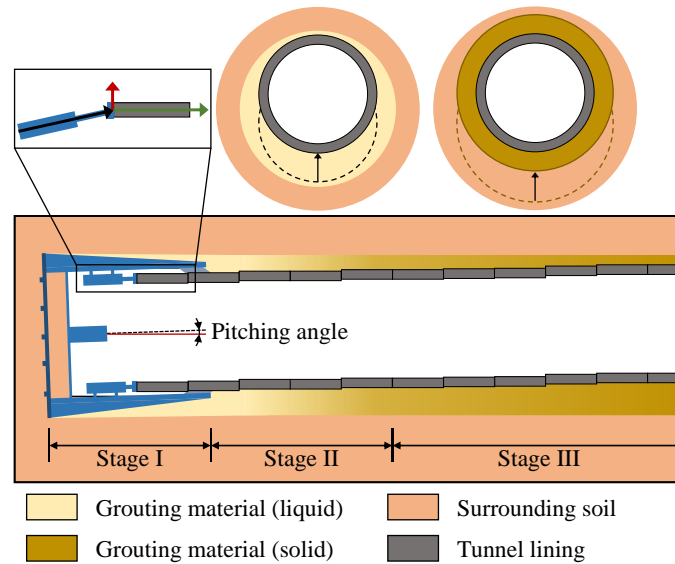


**Figure 1.** Process of segment floating.

In stage II, when the assembled segment is released from the shield machine tail, the grouting material remains in a liquid state. The segment is subjected to great buoyancy if it is warped by the liquid grouting material. Many researchers calculated the buoyancy with the assumption that the segment is totally warped by grouting material. However, this assumption proves overly idealistic, as practical scenarios are inherently more complex. The engineer tends to inject a greater volume of grouting material at the top of the segment, while injecting minimal grouting material at the bottom, as a measure to mitigate segment floating. So, the analysis solution based on buoyancy calculation seldom acquires satisfactory results. Those segments warped in liquid grouting material exhibit behavior akin to a cantilever beam subject to distributed load, with the solid grouting material serving as the cantilever side. The deflection of a cantilever beam is influenced by the length of the beam. Similarly, the extent of the liquid grouting material in the longitudinal direction also affects segment floating. The application of double liquid grouting can effectively decrease the setting time of the grouting material, thereby mitigating segment floating.

In stage III, as the grouting material loses its fluidity, the grouting material and the segment form a system. Due to the relatively lower gravity of the system compared to the surrounding excavated soil, the system exhibits upward movement before gradually settling. In Stage III, the segment floating is tightly related to the geological condition and stratum stress.

## 2.2. Parameters related to segment floating

Based on the three stages during segment floating, the parameters related to the segment floating can be divided into geometry parameters, geological parameters, shield excavation parameters, shield moving trajectory parameters, tail grouting parameters, and others. Noted, shield excavation, shield moving trajectory, and tail grouting parameters are collectively referred to as shield operational parameters. Different parameters take major effect at different stages of segment floating. Geometry parameters take effect throughout the floating process, while geological parameters majorly take effect at stage III. Shield excavation and moving trajectory parameters predominantly take effect at Stage I, whereas tail grouting parameters come into play at Stage II. Besides the aforementioned parameters, there are certain other

parameters within the measurements that are effective in controlling segment floating, for example, secondary grouting, emergency sandbag, and change grouting material. Those measurements are costly in time and economy; thus, they are selectively utilized when segment floating reaches a severe level. Those measures do not align with the primary objective of optimization of segment floating, therefore, they are not considered in this work.

The geometry parameters only include the outer diameter ( $D$ ) and the depth of the lining ring ( $H$ ). Noted, the depth refers to the vertical distance between the ground surface and the centre of the lining ring.

The geological parameters should include the physical characteristics of strata above and below the lining ring, as well as the water table. Nevertheless, it is difficult to acquire detailed information about the strata in practice. Previous studies addressing geological parameters have often involved categorizing soils into distinct classifications, which are subsequently fed into the model. The soils are divided into five categories based on unsupervised machine learning, the soil clusters in clustering analysis exactly correspond to five typical soil types in geology [28]. Notably, these soil clusters given by clustering analysis precisely align with five well-recognized geological soil types, namely filling, clay, silt, sand, and rock. The thickness of each soil category is taken as input parameters. The thickness of each soil category is adopted as input parameters of the intelligence model. As aforementioned, this study considers the strata both above and below the lining ring and the water table. Following the method, a total of 11 geological parameters are considered in this paper.

The shield operational parameters related to segment floating are given in Table 1. The shield excavation parameters primarily concern the cutter head and the shield shell. The cutter head and the shield shell are predominantly positioned ahead of the assembled segment, yielding the early activation of the shield excavation parameters. Conversely, the grouting material majorly takes effects after the assembly of the segment, contributing to the hysteretic nature of tail grouting parameters. The shield operational parameters are normalized before feeding into deep learning models. Especially for the moving trajectory, the relative value is more important compared to the absolute value.

**Table 1.** Shield operational parameters related to segment floating.

Parameter category	Parameter	Unit	Notation
Shield excavation parameters	Face pressure	bar	$F_p$
	Torque	kN·m	$T_o$
	Thrust	kN	$T_h$
	Rotational speed	rpm	$R_s$
	Penetration rate	mm/min	$P_r$
Moving trajectory parameters	Pitching angle	°	$\theta$
	Yawing angle	°	$\phi$
	Rolling angle	°	$\psi$
Tail grouting parameters	Grouting pressure A of $i$ th grouting pipe	bar	$G_p-A_i$
	Grouting pressure B of $i$ th grouting pipe	bar	$G_p-B_i$
	Grouting volume A of $i$ th grouting pipe $i$	m <sup>3</sup>	$G_v-A_i$
	Grouting volume B of $i$ th grouting pipe	m <sup>3</sup>	$G_v-B_i$

Note:  $i$  represents the different tail grouting pipes which are evenly installed at the shield tail.

Different from the geometrical and geological parameters, shield operational parameters of several tunnel rings are simultaneously taken into account when predicting the segment floating of a single tunnel ring. The geometrical and geological parameters typically exhibit minimal variation between two adjacent tunnel rings, while the shield operation between such rings may vary significantly. When predicting the segment floating of a tunnel ring, considering the effect of the cantilever beam, the shield operational parameters of two preceding tunnel rings, the predicted tunnel ring, and two subsequent tunnel rings should be simultaneously considered. In this work, the shield operational parameters of five adjacent tunnel rings are simultaneously adopted as input parameters.

### 3. Knowledge-based intelligence method

#### 3.1. Prior knowledge in controlling segment floating

Excessive segment floating will result in segment dislocation, crack, and leakage. Therefore, it is necessary to effectively control the segment floating. As aforementioned, the geometry, geological, and shield operational parameters are related to the segment floating. The geometry and geological parameters are predetermined during the design phase of the tunnel. Consequently, shield operators are tasked with adjusting shield operational parameters effectively to mitigate excessive segment floating. In practice, certain shield operational parameters are determined based on other control targets rather than solely focusing on mitigating segment floating, for example, shield excavation efficiency, stability of tunnel face, and tunnel trajectory alignment. The influence extents of the shield operational parameters on those control targets are different. Moreover, some shield operational parameters, such as thrust and torque [28], are not directly determined by the shield operator. Instead, those parameters are influenced by both the shield operator's decisions and the characteristics of the surrounding soil. In this paper, the parameters directly determined by the shield operator are called active control parameters. Conversely, parameters determined as a result of the active control parameters are referred to as passive response parameters. According to their control targets and whether they are determined by shield operators, the shield operational parameters have been categorized into four groups, as shown in Table 2.

**Table 2.** Shield operational parameters.

Target	Segment floating	Other control targets
Active control parameters	Grouting volume A of <i>i</i> th grouting pipe, grouting volume B of <i>i</i> th grouting pipe	Face pressure, rotational speed, penetration rate, pitching angle, yawing angle, and rolling angle
Passive response parameters	Grouting pressure A of <i>i</i> th grouting pipe, grouting pressure B of <i>i</i> th grouting pipe	Torque, thrust

Generally, shield machines offer two control modes for the tail grouting: flow mode and pressure mode. In flow mode, the grouting pipeline maintains a consistent flow rate during shield advancing. As shown in Figure 2, the grouting volume increases linearly, while the grouting pressure fluctuates due to variations in the surrounding soil conditions. Therefore, in flow mode, the grouting volume serves as an active control parameter, while the grouting pressure functions as a passive response parameter. In pressure mode, grouting commences when the grouting pressure falls below the predefined minimum threshold, and ceases once the grouting pressure surpasses the predefined maximum threshold. So in

pressure mode, grouting pressure and grouting volume are active control parameters and passive response parameters, respectively. In this work, the shield machine in the studied project adopted flow mode. Consequently, the segment floating is controlled by adjusting the grouting volume. Meanwhile, grouting pressure serves as the passive response parameter. For the other control targets, face pressure, rotational speed, penetration rate, pitching angle, yawing angle, and rolling angle are the active control parameters, while thrust and torque are the passive response parameters.

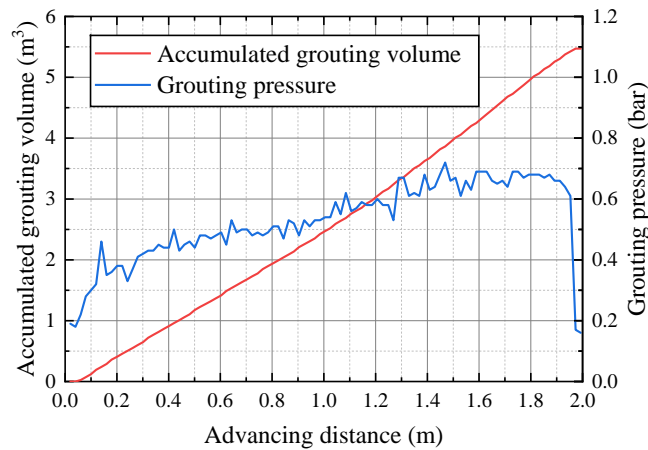


**Figure 2.** Grouting volume and grouting pressure under flow mode.

To facilitate the following analysis, the related parameters are divided into six groups: geometrical parameters, geological parameters, active control parameters for controlling segment floating, active control parameters for other control targets, passive response parameters for controlling segment floating, and passive response parameters for other control targets. The notations of the different parameter groups are given in Table 3.

**Table 3.** Notations of different parameter groups.

Parameter group	Notation	Parameters
Geometrical parameters	$Gm$	Depth, tunnel diameter
Geological parameters	$Gl$	The thickness of each soil category and water table
Active control parameters for controlling segment floating	$Asf$	Pitching angle, grouting volume A of $i$ th grouting pipe, grouting volume B of $i$ th grouting pipe
Active control parameters for other control targets	$Ao$	Face pressure, rotational speed, penetration rate, horizontal deviation, and vertical deviation
Passive response parameters for controlling segment floating	$Psf$	Grouting pressure A of $i$ th grouting pipe, grouting pressure B of $i$ th grouting pipe
Passive response parameters for other control targets	$Po$	Torque, thrust

The mechanism of segment floating control is shown in Figure 3. Initially, shield operators decide  $Ao$  and  $Asf$  based on their engineering experience. Then, the interaction between the shield machine and surrounding soil yields  $Po$  based on  $Ao$ ,  $Gm$ , and  $Gl$ . Similarly, the interaction between the segment and surrounding soil yields  $Po$  based on  $Asf$ ,  $Gm$ , and  $Gl$ . Next, the interaction between the segment, shield machine, and surrounding soil determines the segment floating according to all the parameters. The three interactions represent different physical principles governing shield tunnelling. Models aimed at the prediction or the control of segment floating must obey those three physical principles to achieve great performance.

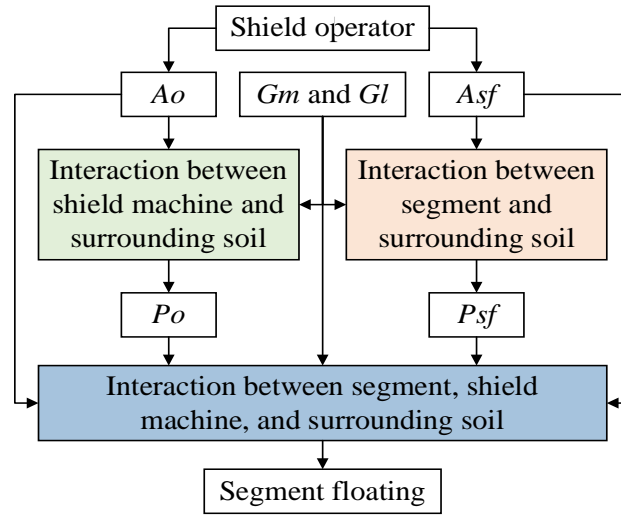


**Figure 3.** Mechanism of controlling segment floating.

3.2. Framework of proposed intelligence method

In this work, a knowledge-based intelligence method for controlling segment floating is developed, with its framework illustrated in Figure 4. The intelligence method consists of three models, each aligned with one of the three interactions inherent in the mechanism of controlling segment floating introduced in Section 3.1. The three models include the segment floating prediction model, the torque and thrust prediction model, and the grouting pressure prediction model. In the proposed intelligence method,  $A_o$  is still determined by the shield operator or other algorithms. Aiming at the interaction between the shield machine and the surrounding soil, the torque and thrust prediction model is developed to predict  $P_o$  by feeding  $G_m$ ,  $G_l$ , and  $A_o$ . Different from  $A_o$ ,  $A_{sf}$  is determined by the optimizer. The grouting pressure prediction model is established to predict the  $P_{sf}$  by feeding  $G_m$ ,  $G_l$ , and  $A_{sf}$ . Then,  $G_m$ ,  $G_l$ ,  $A_o$ ,  $A_{sf}$ ,  $P_o$ , and  $P_{sf}$  are fed into the segment floating prediction model to predict the segment floating. The predicted segment floating is used by the optimizer to iteratively update  $A_{sf}$ . If the predicted segment floating fails to meet specified control requirements, the grouting pressure prediction model, the segment floating prediction model, and the optimizer will continue to iterate until satisfactory  $A_{sf}$  is given. The shaded area in Figure 4 represents the iterative calculation process aimed at minimizing the predicted segment floating.

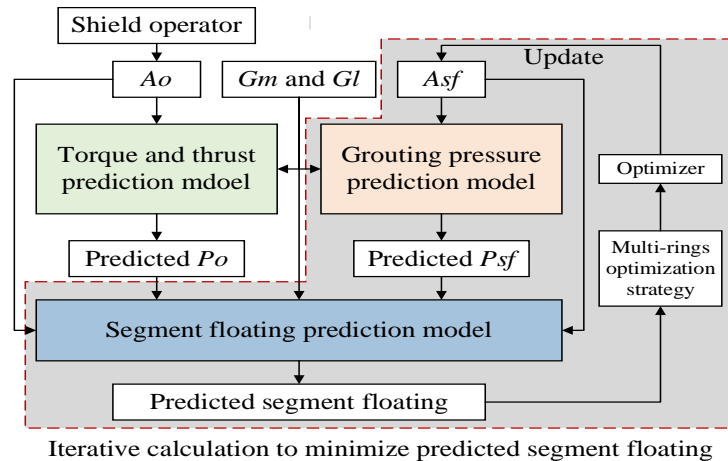


**Figure 4.** Framework of proposed intelligence method of segment floating.

Optimizers are algorithms aiming at finding the best solution to an optimization problem from a set of possible solutions, typically achieved by minimizing or maximizing a certain objective function. An optimizer consists of three essential components: decision variables, objective functions, and constraints. The objective function reflects the relationship between the decision variable and the quantity which is minimized or maximized. Decision variables are parameters that the optimizer can modify in the objective function. Constraints are used to regulate the range of decision variables, typically given based on the physical significance of the optimization problem. In the proposed intelligence method of segment floating,  $Asf$  serves as the decision variable. The grouting pressure prediction model and the segment floating prediction model constitute the object function.  $Gm$ ,  $Gl$ , and predicted  $Po$  are considered fixed parameters in the objective function. Moreover, to address the conflicts between the optimization results of adjacent rings, a multi-rings optimization strategy is developed in Section 3.4.

In engineering practice, the proposed intelligence method will recommend the tail grouting parameters of each ring, and shield operator can adjust the shield machine according the recommended value.

In engineering practice, the proposed intelligent method is designed to recommend optimal tail grouting parameters for each ring. Shield operators can then adjust the shield machine settings based on these recommended values to ensure optimal performance. Other shield operational parameters may be suggested by similar intelligent methods.

### 3.3. Segment floating prediction model and auxiliary model

#### 3.3.1. Segment floating prediction model

In the segment floating prediction model, both Convolution Neural Network (CNN) and Deep Neural Network (DNN) are adopted. DNN is employed to extract the latent information from the geometry and geological parameters. CNN is used to extract the latent information from shield operational parameters. To improve the prediction accuracy, two techniques are adopted: dropout and residual network (ResNet).

The framework of the segment floating prediction model is shown in Figure 5. Considering the spatial and temporal characteristics of the shield operational parameter, one ResNet processes the shield excavation and moving trajectory parameters, while the other ResNet processes the tail grouting parameters. The geometrical and geological parameters constitute an array with a size of  $1 \times 13$ . The shield excavation and moving trajectory parameters for 5 tunnel rings are encoded as an array of size  $5 \times 8$ . Additionally, the tail grouting parameters of 5 tunnel rings are encoded as an array of size  $5 \times 4 \times 8$ . The features provided by DNN, CNN 1, and CNN 2 are reshaped and then concatenated, yielding an array of size  $1 \times 48$ . Then the array is processed by a decoder, which then outputs the predicted segment floating.

#### 3.3.2. Torque and thrust prediction model

The torque and thrust prediction model is employed for forecasting both thrust and torque, utilizing geometrical parameters, geological parameters, active control parameters for other control targets, and historical data for other control targets. The schematic representation of this model is illustrated in Figure 6, comprising an input layer, hidden layer, output layer, and loss layer. In this illustration, rectangles and rounded rectangles represent tensors and networks, respectively.

In the input layer, four tensors are generated from the input parameters. Notably, historical data are employed to extract latent information related to the shield status. The hidden layer employs encoder-decoder architectures. Within the encoder block, the input tensor generated from historical data undergoes processing through a bidirectional gated recurrent neural network (Bi-GRU) and a projection. The resulting output is concatenated with other input tensors. Subsequently, a DNN with a skip connection is employed to extract latent information from the concatenated tensor, thereby output the encoded latent feature. In the decoder block, both the torque decoder and thrust decoder leverage the encoded latent feature to predict the corresponding torque and thrust values, respectively. Subsequently, in the loss layer, individual losses for torque and thrust are calculated. These losses are summed up to yield the total loss, which is used to update the trainable parameters in both the encoder and decoder blocks. The proposed model considers both the similarities and differences in predictions of thrust and torque. The encoder block is designed to extract the shared latent information present in the predictions of both torque and thrust. Meanwhile, the torque and thrust decoders are tailored to capture the unique latent information and specialized characteristics associated with predicting torque and thrust, respectively.

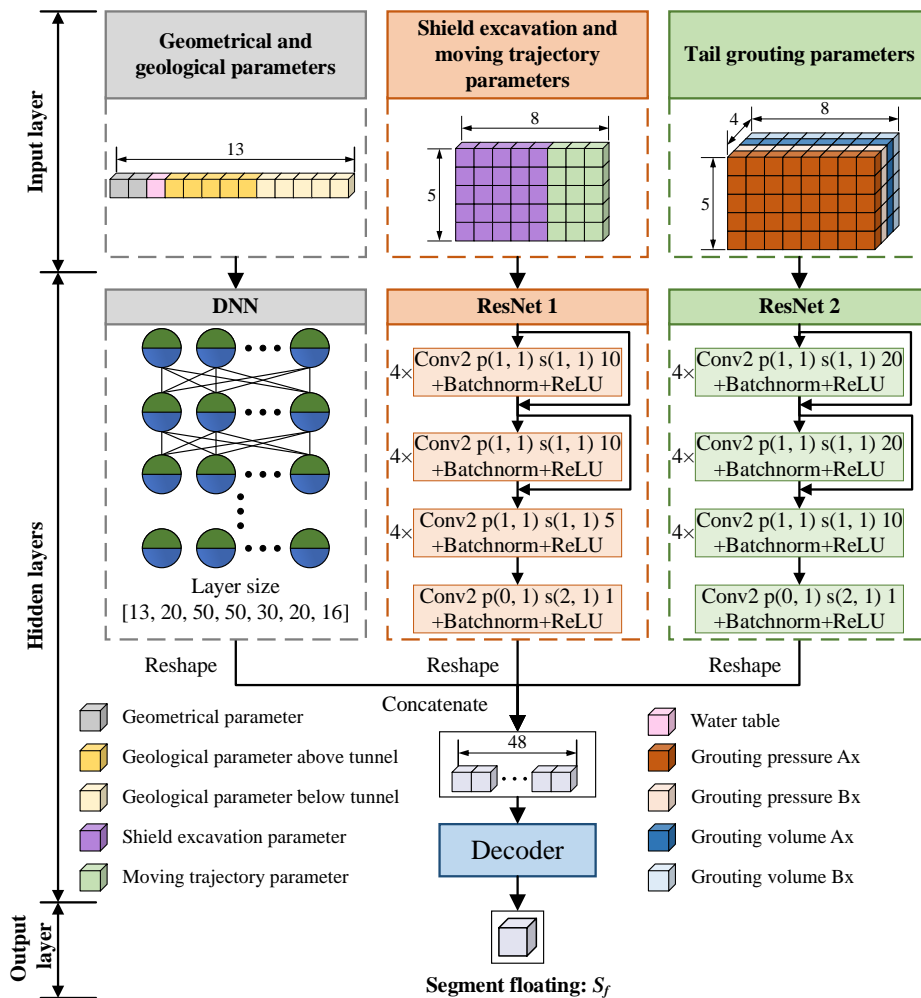


Figure 5. Framework of segment floating prediction model.

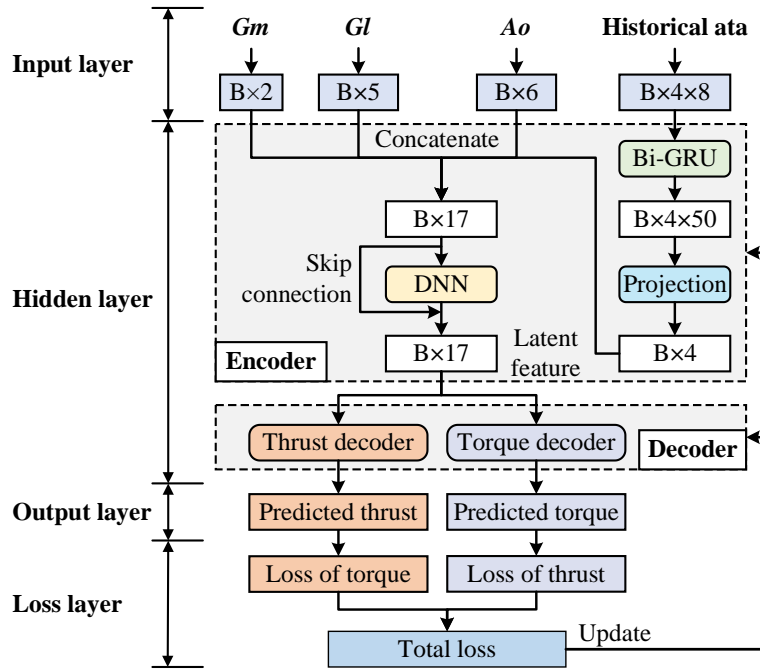


Figure 6. Torque and thrust prediction model.

3.3.3. Grouting pressure predicting model

The framework of the grouting pressure prediction model, as illustrated in Figure 7, is employed to forecast the grouting pressure by utilizing parameters such as the grouting volume parameters ( $Gv-Ai$  and  $Gv-Bi$ ), geological parameters ( $Gl$ ), and tunnel diameter ( $D$ ). Noted, the geological parameters here are the summation of geological parameters above and below the lining ring.

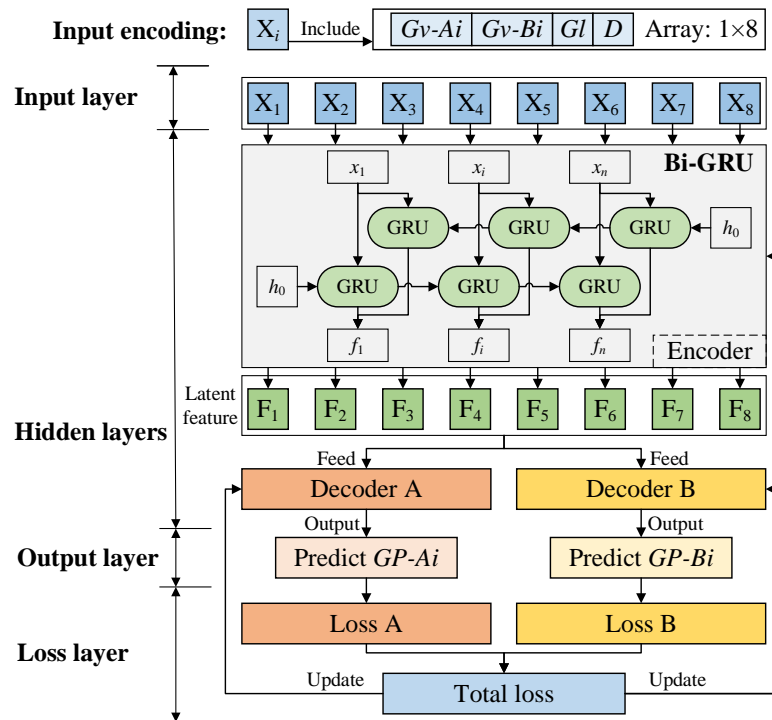


Figure 7. Grouting pressure prediction model.

As depicted in Figure 7, each input token ( $X_i$ ) represents an array with a size of  $1 \times 8$ , corresponding to a single grouting pipe. The grouting pressure prediction model adopts an encoder-decoder framework. A Bi-GRU is chosen as the encoder to extract latent information from the input parameters and generate the latent features ( $F_i$ ). The Bi-GRU is capable of considering the spatial characteristics of various grouting pipes and producing features for each individual grouting pipe. Subsequently, decoder A and decoder B are employed to handle the features of each grouting pipe and generate the corresponding grouting pressures. These decoders establish the relationship between the latent feature and the grouting pressure of each pipe. Decoder A and decoder B are designed to account for the specificities in predicting  $GP-A_i$  and  $GP-B_i$ , respectively. The loss layer operates similarly to that of the thrust and torque prediction model. Table 4 gives the hyperparameter in the grouting pressure prediction model.

**Table 4.** Hyperparameter in grouting pressure prediction model.

Network name	Hyperparameters	Value
Bi-GRU	Hidden size	50
	dropout	0.1
Decoder A	Network size	[50, 50, 50, 50, 50, 50, 25, 10, 1]
Decoder B	Network size	[50, 50, 50, 50, 50, 50, 25, 10, 1]

### 3.4. Multi-rings optimization strategy

In the optimization, the decision variable includes the parameters for five rings. However, the segment floating prediction model only predicted the segment floating for a single ring. This discrepancy results in the conflict between the optimization results of two near rings as shown in Figure 8. Each panel represents a tunnel ring, with a black dot indicating the tunnel ring selected as the optimization target. When the segment floatings of two adjacent tunnel rings are respectively optimized, conflicts arise in the optimization results for four tunnel rings. The pane in green represents the tunnel ring whose optimization result is in conflict.

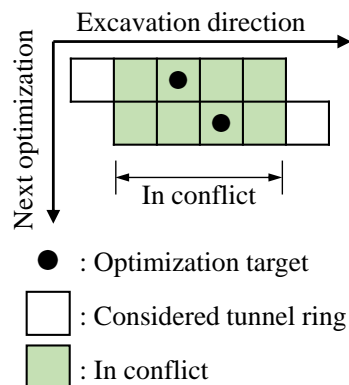


**Figure 8.** Conflict in single ring optimization.

To address this conflict, we proposed a multi-ring optimization strategy that considers the segment floatings of multiple rings. Because those optimization algorithms introduced in Section 3 can only deal with one optimization target, we take the weight summation of those segment floatings, as shown in Equation 1.

$$sf = \sum_{i=1}^m \gamma^{i-1} \cdot sf_i \quad (1)$$

Where  $sf$  is the weighted summation;  $m$  is the number of tunnel rings considered as optimization target;  $sf_i$  is the segment floating of the  $i$ th tunnel ring;  $\gamma$  is the weight factor,  $\gamma$  is smaller than 1. As shown in Figure 9, panes in a row represent the tunnel rings whose  $Asfs$  are fed into the segment floating prediction model. A pane in blue represents a tunnel ring whose  $Asf$  is excluded from the decision variable and determined during the last optimization.  $k$  denotes the number of the tunnel rings whose  $Asfs$  are excluded from the decision. The pane in dark green represents that tunnel ring whose  $Asf$  is determined during this optimization. On the contrary, a pane in light green represents that optimized  $Asf$  is overlapped and adopted as the initial value in the next optimization.

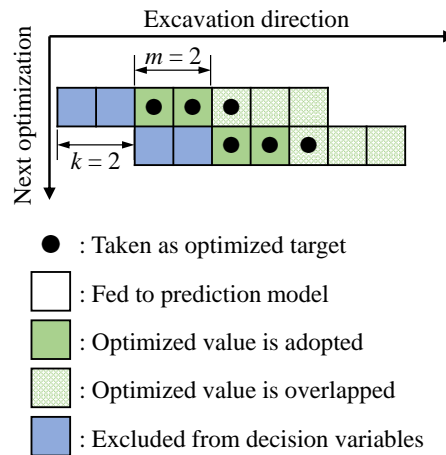


**Figure 9.** Multi-rings optimization strategy.

Along the excavation direction, the segment floating of the latter ring is assigned a smaller weight. The weight summation ensures that the optimization primarily focuses on the former ring, as the latter ring will be optimized in the subsequent optimization.

Nowadays, there are many different types of optimization algorithms, each algorithm has its strengths and weaknesses. Considering the continuity of the decision variable, optimization can be categorized into two main types: continuous optimization problems and discrete optimization problems. The optimization of the control parameters is a typical continuous optimization problem. Stochastic Gradient Descent (SGD), Particle Swarm Optimization (PSO), and Simulated Annealing (SA) are particularly suitable for the continuous optimization problem.

**Stochastic gradient descent algorithm**-Stochastic gradient descent (SGD) is a variant of the gradient descent algorithm. The gradient descent algorithm and its variants are widely used in machine learning and deep learning. The gradient descent algorithm is an iterative method that aims to minimize a differentiable function, often associated with the cost or loss function. The decision variable is updated based on the gradient of the loss function. The concept is analogous to a drop of water sliding down a surface, moving in the direction of the steepest decrease until reaching the bottom. To improve the calculation efficiency, SGD is developed. SGD calculates the gradient using a random subset of the data instead of all the data. The introduction of randomness in gradient computation helps SGD escape the local minima and find true minima.

**Simulated Annealing**-Simulated Annealing (SA) is a stochastic optimization algorithm inspired by the annealing process in metallurgy. The annealing process includes heating a material and then slowly lowering the temperature to decrease defects, thus minimizing the system energy. When finding the values of decision variables corresponding to the global minima of the objective function, SA accepts all new values that lower the objective function, but also, with a certain probability, values that raise the objective function. By accepting values that raise the objective function, SA avoids being trapped in local minima and can explore globally for more possible solutions.

**Particle swarm optimization**-Particle swarm optimization (PSO) is one of the bio-inspired algorithms based on simulating the movement of a flock of birds. PSO is a straightforward method for finding optimal solutions within a search space. Unlike other optimization algorithms, it requires only the objective function and does not rely on gradients or differential forms of the objective. Additionally, it has only a few hyperparameters to adjust. PSO optimizes a problem by iteratively improving candidate solutions, called particles, based on a quality measure. Particles move through the search space, influenced by their own best-known positions and the best-known positions discovered by others, gradually guiding the swarm toward optimal solutions. It cannot be proved that the real global optimal solution can be found by PSO. However, the solution found by PSO is quite close to the global minimum.

#### 4. Case study

In this work, the geometry parameter, geological parameter, shield operational parameter, and segment floating during the construction of a shield tunnel project in China are collected to evaluate the segment floating prediction model and the proposed intelligence method. The tunnel spans approximately 7.3 km in length. The tunnel project is subdivided into two primary sections by the middle shaft: the north tunnel section and the south tunnel section. The north and south tunnel sections each span about 2.6 km and 4.8 km in length, respectively. The shield tunnel has an outer diameter of 16.07m and transverses water-rich sand layers. The combination of the large diameter and the water-rich sand layers exacerbates the severity of the segment floating in the project. The buried depth varies from 11.05 m to 50.1 m. The geological profile of the tunnel is shown in show Figure 10. The statistical distribution of partial geometry and shield operational parameters are given in Table 5. Additionally, the value distribution of segment floating is shown in Figure 11.

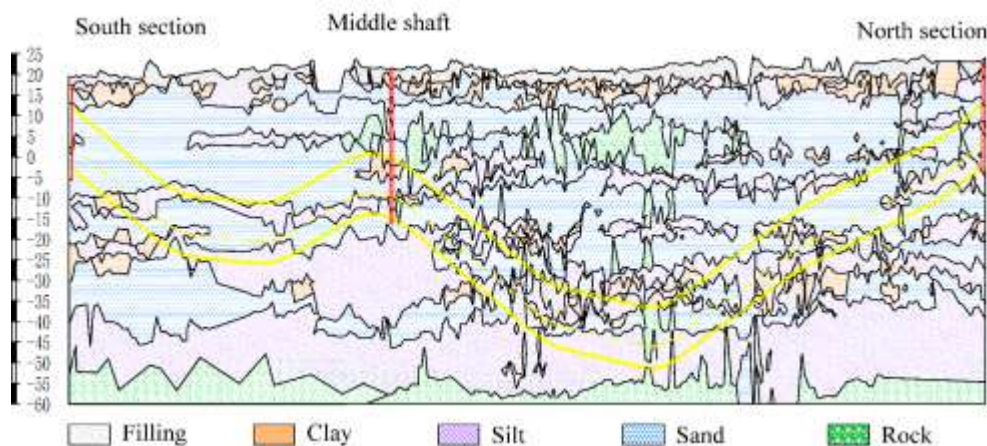


**Figure 10.** Geological profiles.

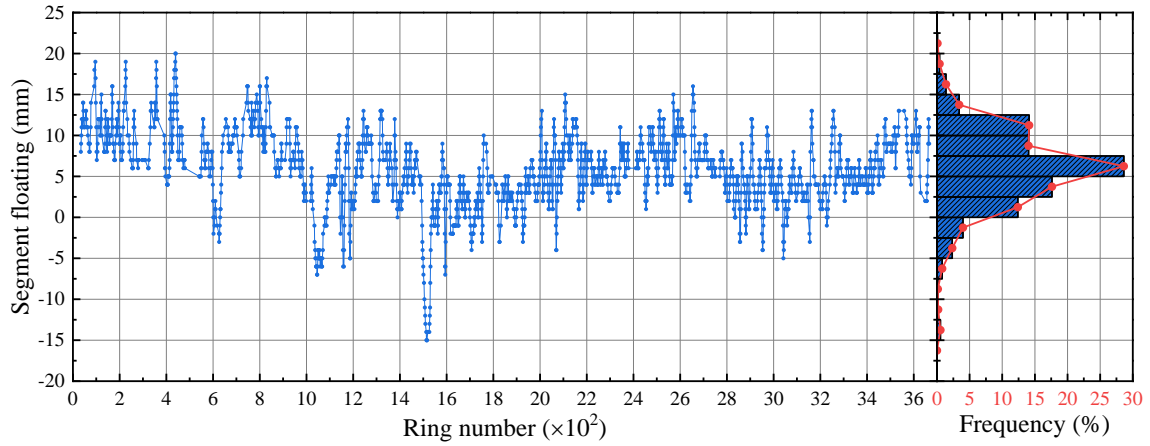


**Figure 11.** Value distribution of segment floating.

**Table 5.** Descriptive statistical values of parameters.

Parameter	Maximum	Minimum	Mean	Standard deviation
Depth	50.10	11.05	32.90	10.91
Face pressure	7.22	1.57	4.87	1.49
Rotational speed	1.42	0.65	1.06	0.12
Penetration rate	50.99	4.51	26.51	6.35
Torque	38310.00	3100.67	13706.81	6315.05
Thrust	242691.20	57718.76	122826.42	38013.26
Pitching angle	1.54	-1.79	0.02	1.03
Yawing angle	0.24	-0.11	0.07	0.07
Rolling angle	0.46	-0.17	-0.01	0.04

## 5. Analysis

### 5.1. Analysis of segment floating prediction model

When predicting the segment floating of a tunnel ring, the shield operational parameters from five adjacent tunnel rings are fed into the segment floating prediction model simultaneously. To evaluate the improvement achieved by considering five rings, a comparative model is constructed. The comparative model solely incorporates the shield operational parameters of the predicted tunnel ring and is compared with the proposed segment floating prediction model. The prediction results obtained from both the proposed segment floating prediction model and the comparative model are shown in Figure 12. The performances of models are evaluated using Mean Absolute Error (*MAE*), Root Mean Square Error (*RMSE*), and Correlation Coefficient ( $R^2$ ). The equations for *MAE*, *RMSE*, and  $R^2$  are shown as follows.

$$MAE = \frac{1}{n} \sum_{i=1}^n |m_i - p_i| \quad (2)$$

$$RMSE = \sqrt{\frac{1}{n} \sum_{i=1}^n (m_i - p_i)^2} \quad (3)$$

$$R^2 = \frac{\sum_{i=1}^n (p_i - m_i)^2}{\sum_{i=1}^n (\bar{m} - m_i)^2} \quad (4)$$

where  $m_i$  and  $p_i$  are the measured settlement and predicted settlement, respectively;  $\bar{m}$  and  $\bar{p}$  are the average value of the measured settlement and predicted settlement, respectively; and  $n$  is the total number of monitoring points.

It can be seen in Figure 12 that the proposed segment floating prediction model gives better prediction results. Specifically, the proposed model achieves an  $R^2$  value of 0.903, outperforming the comparative model which attains an  $R^2$  value of 0.838. Similarly, the  $MAE$  and  $RMSE$  of the proposed segment floating prediction model are smaller than those of the comparative model. According to the  $MSE$ , the prediction accuracy of the proposed prediction model increases by 30%. The comparison proves the impact of considering shield operational parameters from five rings on the prediction accuracy of the proposed segment floating prediction model.

To investigate the improvement achieved by considering shield operational parameters from five rings, the feature relevance explanation technique is adopted to assess the inputs' contributions or sensitivity toward the output. Global sensitivity analysis (GSA), a typical model-agnostic method, is a feature relevance explanation technique based on the perturbation of the input. In this study, the total-order index, denoted as  $ST_i$ , is employed.  $ST_i$  quantifies the contribution of the input variable  $X_i$  to the output variance. A larger  $ST_i$  indicates a greater contribution. The GSA results of shield operational parameters are shown in Figure 13. In the context of this study, 'n' denotes the serial number of the predicted tunnel ring. Tunnel rings n-2, n-1, n, n+1, and n+2 refer to the five tunnel rings whose shield operational parameters are fed into the model when predicting the segment floating of tunnel ring n. The vertical axis in Figure 13 illustrates the different shield operational parameters. Noted,  $ST_i$  of grouting pressure A represents the mean of  $ST_i$  values for all pipes' grouting pressure  $A_i$ ; similarly, this applies to the other tail grouting parameters.

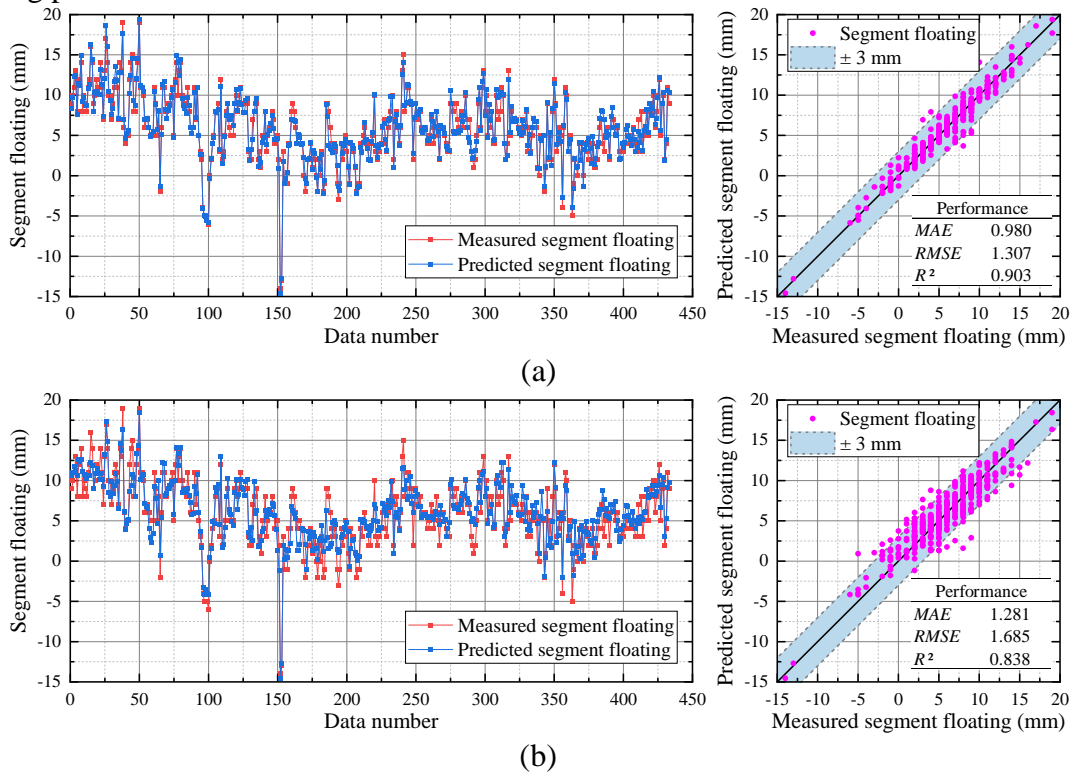


**Figure 12.** Value distribution of predicted segment floating: (a) Segment floating prediction model considering multiple rings; (b) Segment floating prediction model considering single ring.

To investigate the improvement achieved by considering shield operational parameters from five rings, the feature relevance explanation technique is adopted to assess the inputs' contributions or sensitivity toward the output. Global sensitivity analysis (GSA), a typical model-agnostic method, is a feature relevance explanation technique based on the perturbation of the input. In this study, the total-order index, denoted as  $S_{Ti}$ , is employed.  $S_{Ti}$  quantifies the contribution of the input variable  $X_i$  to the output variance. A larger  $S_{Ti}$  indicates a greater contribution. The GSA results of shield operational parameters are shown in Figure 13. In the context of this study, 'n' denotes the serial number of the predicted tunnel ring. Tunnel rings  $n-2$ ,  $n-1$ ,  $n$ ,  $n+1$ , and  $n+2$  refer to the five tunnel rings whose shield operational parameters are fed into the model when predicting the segment floating of tunnel ring  $n$ . The vertical axis in Figure 13 illustrates the different shield operational parameters. Noted,  $S_{Ti}$  of grouting pressure A represents the mean of  $S_{Ti}$  values for all pipes' grouting pressure  $A_i$ ; similarly, this applies to the other tail grouting parameters.

As shown in Figure 13, the contribution of shield excavation parameters generally focuses on the rings  $n-2$  and  $n-1$ . This is because of the early activation of the shield excavation parameters. The contribution of tail grouting parameters focuses on the ring  $n-2$ ,  $n-1$ , and  $n$ , attributed to the hysteretic nature of tail grouting parameters. This phenomenon proves that the proposed segment floating prediction model effectively considers the spatial and temporal characteristics of the shield operational parameters, leading to improved prediction accuracy. The comparative model overlooks the shield operational parameters of rings  $n-2$ ,  $n-1$ ,  $n+1$ , and  $n+2$ , which have great contributions to the segment floating prediction. Consequently, the comparative model yields inferior predictions due to this oversight.

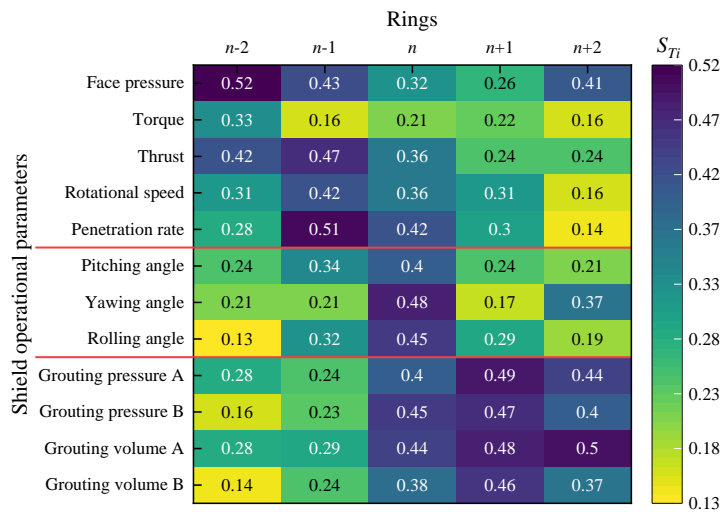


**Figure 13.** Global sensitivity analysis of shield operational parameters.

### 5.2. Analysis of proposed intelligence method

In this section, we analyze the influence of the optimization algorithm and the multi-ring optimization algorithm strategy on the performance of the proposed intelligence method. We constructed and compared intelligence methods utilizing different optimization algorithms and multi-ring strategies. Those intelligence methods are evaluated based on several criteria including the mean ( $\mu$ ), standard deviation ( $\sigma$ ), maximum ( $max$ ), and minimum ( $min$ ) of the optimized result. Also, the performances of those models are compared with the filed data from the studied project.

5.2.1. Optimization algorithms

The distribution of filed data and the optimization result obtained with different optimization algorithms are shown in Figure 14. Those optimization algorithms include Stochastic Gradient Descent (SGD), Particle Swarm Optimization (PSO), and Simulated Annealing (SA). Additionally, the mean ( $\mu$ ), standard deviation ( $\sigma$ ), maximum ( $max$ ), and minimum ( $min$ ) are also given in Figure 14 and summarized in Table 6. In terms of mean, the optimized results obtained with those optimization algorithms outperform the field data. Among the optimization results obtained with different optimization algorithms, SGD gives the best performance. The mean and standard deviation of optimization results with SGD are smaller than those of PSO and SA. Moreover, SGD gives the smallest data range when compared to the optimization results and field data. Among the three optimization algorithms, PSO gives the worst optimization results. Although there is an improvement in the mean compared to the field data, the standard deviation with PSO is even larger than that of the field data. This discrepancy can be attributed to PSO's tendency to become trapped in local minima, thereby hindering its ability to achieve optimal results.

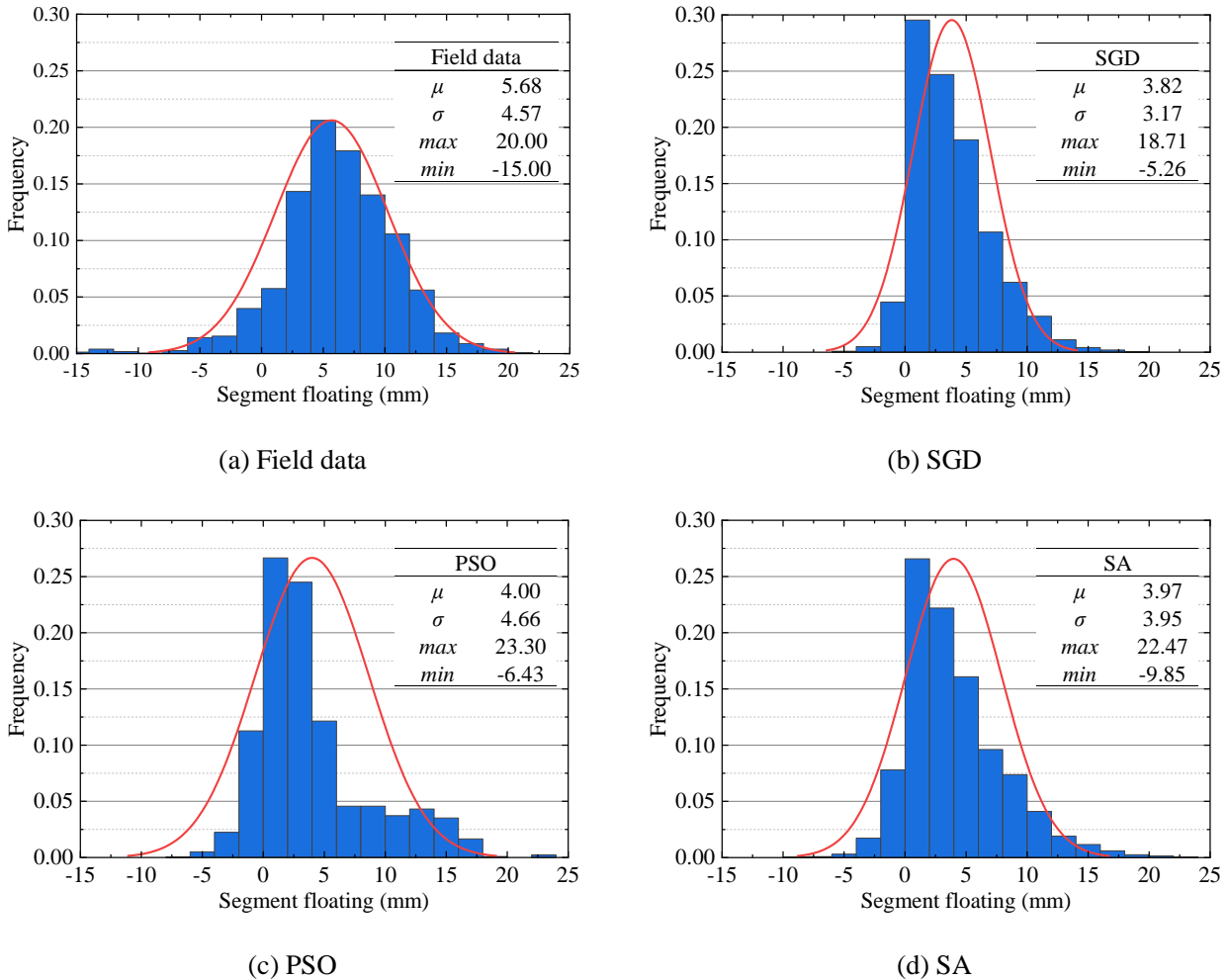


**Figure 14.** Comparison between three optimization algorithms and filed data.

**Table 6.** Summary of comparison between three optimization algorithms and field data.

	Mean ( $\mu$ )	Standard deviation ( $\sigma$ )	Maximum ( $max$ )	Minimum ( $min$ )
Field data	5.68	4.57	20.00	-15.00
SGD	3.82	3.17	18.71	-5.26
PSO	4.00	4.68	23.30	-6.43
SA	3.97	3.95	22.47	-9.85

5.2.2. Analysis of multi-ring optimization strategy

To investigate the influence of the multi-ring optimization strategy on the performance of the proposed intelligence method, we design 5 parameter configurations for the multi-ring optimization strategy. Table 7 illustrates the  $m$ ,  $l$ , and schematic diagram for each parameter configuration. Subsequently, we construct five intelligence methods utilizing these parameter configurations, with SGD selected as the optimization algorithm.

The mean and standard deviation of the optimization result and the computation cost are shown in Figure 15. Here, the computation cost refers to the time required to complete the optimization of all tunnel rings. Across configurations 1 to 5, there is a discernible decrease in both the mean and standard deviation, coupled with an increase in computation cost. Especially, when comparing configuration 2 with 3, the decrease in  $l$  leads to declines in both the mean and standard deviation. Similarly, when comparing configuration 3 with 5, the increase in the  $m$  results in decreases in the mean and standard deviation. As for the computation cost, a smaller  $l$  leads to more iterations in the multi-ring optimization strategy, while a smaller  $m$  reduces the computation cost of each iteration. Therefore, the decreases in both  $l$  and  $m$  contribute to an increase in computation cost. Considering the balance of the computation cost and optimization performance, the optimal parameters configuration of the multi-ring optimization strategy is  $m = 3$  and  $l = 2$ .

**Table 7.** Different configurations of parameters in multi-ring optimization strategy.

No.	$m$	$l$	Schematic diagram
1	1	1	
2	2	2	
3	2	1	
4	3	2	
5	3	1	

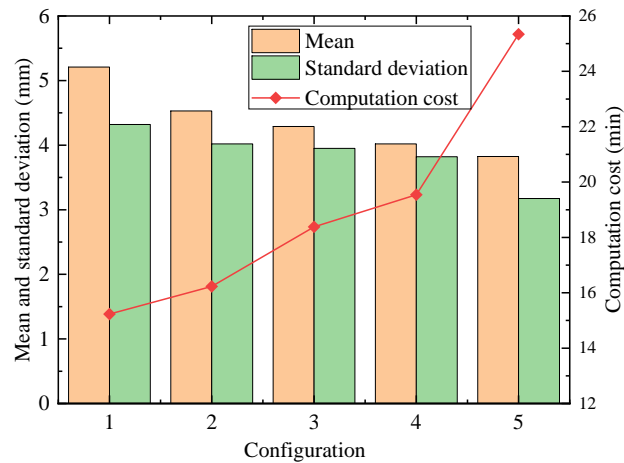


**Figure 15.** Performance of multi-step optimization algorithms with different parameter configurations.

## 6. Conclusion

In this work, we proposed a knowledge-based intelligence method for controlling segment floating based on adjusting and optimizing shield tail grouting parameters. Based on prior knowledge in controlling segment floating, we construct the framework of the intelligence method, comprising a main model and two auxiliary models. The main model, segment floating prediction model, is the basis in the knowledge-based intelligence method. Additionally, a multi-ring optimization strategy is designed to address the conflict between the optimization results of adjacent rings. Based on the case study of an engineering project, the following conclusions can be drawn:

- (1) The proposed segment floating prediction model can predict the segment floating well. Compared to the prediction model considering only the shield operational parameters of the predicted tunnel ring, the proposed prediction model exhibits a notable 30% improvement in prediction accuracy.
- (2) The GSA result of the prediction model implies the early activation of the shield excavation parameters and the hysteretic nature of tail grouting parameters.
- (3) Intelligence methods with optimization algorithms SDG, PSO, and SA successfully optimize the segment floating. The intelligence method with SGD yields the most favorable the best optimization result. Conversely, PSO gives the worst optimized result due to the tendency to be trapped in local minima.
- (4) The multi-ring optimization strategy addresses the conflict between the optimized results of adjacent tunnel rings. Considering the balance of the computation cost and optimization performance, the optimal parameters configuration of the multi-ring optimization strategy is  $m = 3$  and  $l = 2$ .

In the future, we plan to continuously collect data from various projects to enhance the generalization capability of the proposed method. Additionally, the three components can be further optimized using a multi-task learning network. The optimization process may also be refined through the application of sensitivity analysis techniques [30].

## Acknowledgments

The authors gratefully acknowledge the financial support by National Key R&D Program of China (Grant Number: 2024YFE0198500) and National Natural Science Foundation of China (Grant Number: U2469207).

## Authors' contribution

Gan Wang: Writing – original draft, Methodology, Conceptualization. Qian Fang: Writing – review & editing, Supervision. Jun Wang: Visualization, Validation, Data curation. Guoli Zheng: Investigation, Formal analysis. Qiming Li: Software, Data curation. Jianying Wei: Writing – review & editing, Methodology.

## Conflicts of interests

The authors declare that they have no conflicts of interest in this paper.

## References

- [1] Liang Y, Zhang J, Lai Z, Huang Q, Huang L. Temporal and spatial distribution of the grout pressure and its effects on lining segments during synchronous grouting in shield tunnelling. *Eur. J. Environ. Civ. Eng.* 2020, 24(1):79–96.
- [2] Geng D, Hu Y, Jiang Y, Wang N, Hu W. Modified calculation model for segment floating in slurry shield tunnel. *J. Perform. Constr. Facil.* 2021, 35(5):04021068.
- [3] Liu X, Yuan D. Mechanical analysis of anti-buoyancy safety for a shield tunnel under water in sands. *Tunn. Undergr. Space Technol.* 2015, 47:153–161.
- [4] Bezuijen A, Talmon AM, Kaalberg FJ, Plugge R. Field measurements of grout pressures during tunnelling of the sophia rail tunnel. *Soils Found.* 2004, 44(1):39–48.
- [5] Talmon AM, Bezuijen A. Simulating the consolidation of TBM grout at Noordplaspolder. *Undergr. Space Technol.* 2009, 24(5):493–499.
- [6] Jin H, Yuan D, Jin D, Wu J, Wang X, *et al.* Shield kinematics and its influence on ground settlement in ultra-soft soil: a case study in Suzhou. *Can. Geotech. J.* 2022, 59(11):1887–1900.
- [7] Jiang Y, Xu Z, Geng D, Dong J, Liao Y. Optimization of grouting material for shield tunnel antifloating in full-face rock stratum in nanchang metro construction in China. *Int. J. Geomech.* 2022, 22(4):04022009.
- [8] Jiang X, Zhu H, Yan Z, Zhang F, Ye F, *et al.* A state-of-art review on development and progress of backfill grouting materials for shield tunneling. *Dev. Built Environ.* 2023, 16:100250.
- [9] Wang G, Fang Q, Du J, Wang J. Semi-analytical solution for internal forces of tunnel lining with multiple longitudinal cracks. *J. Rock Mech. Geotech. Eng.* 2023, 15(8):2013–2024.
- [10] Fang Q, Wang G, Yu F, Du J. Analytical algorithm for longitudinal deformation profile of a deep tunnel. *J. Rock Mech. Geotech. Eng.* 2021, 13(4):845–854.
- [11] Mei Y, Luo Z, Jiang H, Gong H, Hou Y, *et al.* Study on the floating law of metro segments in water-rich sandy silt and silty clay strata. *KSCE J. Civil Eng.* 2022, 26(6):2979–2991.
- [12] Wang G, Fang Q, Wang J, Li Q, Song H, *et al.* Artificial intelligence prediction of surface settlement induced by twin shields tunnelling. *Tunn. Undergr. Space Technol.* 2025;161:106606.
- [13] Wang G, Fang Q, Wang J, Li Q, Zhou M. Ground movement prediction for twin tunnels with minimum total potential energy principle considering volumetric change of soil. *Transp. Geotech.* 2024, 49:101452.
- [14] Fang Q, Wang G, Du J, Liu Y, Zhou M. Prediction of tunnelling induced ground movement in clay using principle of minimum total potential energy. *Tunn. Undergr. Space Technol.* 2023, 131, 104854.
- [15] Wang J, Fang Q, Zheng G, Wang G, Chen J, *et al.* Influences of bit button wear on performance of

- rotary-percussive drilling: MBD-DEM coupling simulation and verification. *J. Rock Mech. Geotech. Eng.* 2025, 17(3):1585–1598.
- [16] Wang J, Fang Q, Wang G, Zheng G, Jin H, *et al.* Semi-supervised recognition of tunnel surrounding rock discontinuities using drilling jumbo data. *Autom. Constr.* 2024, 166:105623.
- [17] Li X, Yao M, Yuan J, Wang Y, Li P. Deep learning characterization of rock conditions based on tunnel boring machine data. *Undergr. Space.* 2023, 12:89–101.
- [18] Ren Y, Huang J, Hong Z, Lu W, Yin J, *et al.* Image-based concrete crack detection in tunnels using deep fully convolutional networks. *Constr. Build. Mater.* 2020, 234:117367.
- [19] Li J, Chen Z, Li X, Jing L, Zhangf Y, *et al.* Feedback on a shared big dataset for intelligent TBM Part I: Feature extraction and machine learning methods. *Undergr. Space.* 2023, 11:1–25.
- [20] Li J, Chen Z, Li X, Jing L, Zhang Y, *et al.* Feedback on a shared big dataset for intelligent TBM Part II: Application and forward look. *Undergr. Space.* 2023, 11:26–45.
- [21] Zhang Q, Hou Z, Huang G, Cai Z, Kang Y. Mechanical characterization of the load distribution on the cutterhead–ground interface of shield tunneling machines. *Tunn. Undergr. Space Technol.* 2015, 47:106–113.
- [22] Zhang Q, Huang T, Huang G, Cai Z, Kang Y. Theoretical model for loads prediction on shield tunneling machine with consideration of soil-rock interbedded ground. *Sci. China Technol. Sci.* 2013, 56, 2259–2267.
- [23] Zhang Q, Qu C, Cai Z, Kang Y, Huang T. Modeling of the thrust and torque acting on shield machines during tunneling. *Autom. Constr.* 2014, 40:60–67.
- [24] Liu X, Li K, Jiang A, Fang Q, Zhang R. Prediction interaction responses between railway subgrade and shield tunnelling using machine learning with sparrow search algorithm. *Transp. Geotech.* 2024, 44:101169.
- [25] Li J, Li P, Guo D, Li X, Chen Z. Advanced prediction of tunnel boring machine performance based on big data. *Geosci. Front.* 2021, 12(1):331–338.
- [26] Tang L, Na S. Comparison of machine learning methods for ground settlement prediction with different tunneling datasets. *J. Rock Mech. Geotech. Eng.* 2021, 13(6):1274–1289.
- [27] Wang G, Fang Q, Wang J, Li Q, Chen J, *et al.* Estimation of load for tunnel lining in elastic soil using physics-informed neural network. *Comput. Aided Civ. Infrastruct. Eng.* 2024, 39(17):2701–2718.
- [28] Wang G. Deep learning-based prediction of steady surface settlement due to shield tunnelling. *Autom. Constr.* 2023, 154:105006.
- [29] Ge S, Gao W, Cui S, Chen X, Wang S. Safety prediction of shield tunnel construction using deep belief network and whale optimization algorithm. *Autom. Constr.* 2022, 142:104488.
- [30] Gu Y, Lu X, Xu Y. A deep ensemble learning-driven method for the intelligent construction of structural hysteresis models. *Comput. Struct.* 2023, 286:107106.